

# 3D Object Detection with a Self-supervised Lidar Scene Flow Backbone

Emeç Erçelik<sup>1\*</sup>, Ekim Yurtsever<sup>2\*</sup>, Mingyu Liu<sup>1,3</sup>, Zhijie Yang<sup>1</sup>, Hanzhen Zhang<sup>1</sup>,  
Pınar Topçam<sup>1</sup>, Maximilian Listl<sup>1</sup>, Yılmaz Kaan Çaylı<sup>1</sup>, Alois Knoll<sup>1</sup>

<sup>1</sup>Chair of Robotics, Artificial Intelligence and Real-time Systems, Technical University of Munich,  
85748 Garching b. München, Germany

<sup>2</sup> Ohio State University, Columbus, OH 43212, USA

<sup>3</sup> Tongji University 201804, Shanghai, China

emeç.ercelik@tum.de, yurtsever.2@osu.edu, mingyu.liu@tum.de, zhijie.yang@tum.de,  
hanzhen.zhang@tum.de, pınar.topcam@tum.de, maximilian.listl@tum.de, kaan.cayl@tum.de,  
knoll@in.tum.de

## Abstract

*State-of-the-art 3D detection methods rely on supervised learning and large labelled datasets. However, annotating lidar data is resource-consuming, and depending only on supervised learning limits the applicability of trained models. Against this backdrop, here we propose using a self-supervised training strategy to learn a general point cloud backbone model for downstream 3D vision tasks. 3D scene flow can be estimated with self-supervised learning using cycle consistency, which removes labelled data requirements. Moreover, the perception of objects in the traffic scenarios heavily relies on making sense of the sparse data in the spatio-temporal context. Our main contribution leverages learned flow and motion representations and combines a self-supervised backbone with a 3D detection head focusing mainly on the relation between the scene flow and detection tasks. In this way, self-supervised scene flow training constructs point motion features in the backbone, which help distinguish objects based on their different motion patterns used with a 3D detection head. Experiments on KITTI and nuScenes benchmarks show that the proposed self-supervised pre-training increases 3D detection performance significantly.*

## 1. Introduction

Lidar promises accurate distance measurement, which is crucial for real-time systems such as 3D perception modules of automated vehicles. Supervised learning methods have dominated benchmarks created for challenging downstream

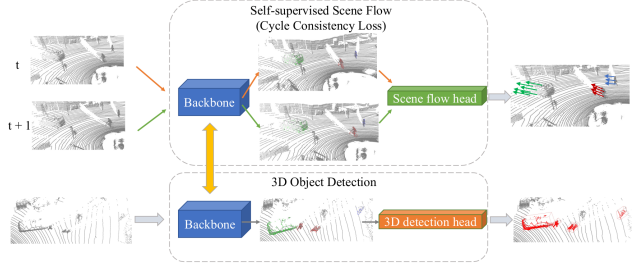


Figure 1: Our main objective is to pre-train a 3D object detection backbone using subsequent point cloud frames within a large unlabeled dataset. To this end, we propose using self-supervised cycle consistency flow loss to train a scene flow estimation network with a shared 3D object detection backbone. We show that this backbone can be used effectively for object detection after fine-tuning on a smaller annotated dataset.

3D vision tasks. However, high-performing models need a copious amount of labelled data for training. Annotating lidar data is labor-intensive and is a bottleneck before real-world deployment.

Recent work showed the importance of self-supervised learning to build large backbones by exploiting the structure of data. For example, the temporal shift in videos can be exploited in contrastive learning strategies [40]. Contrastive methods have also been used with data augmentation [30] for similar purposes. MoCo [15] classifies images in binary form as positive and negative to learn useful representations. Another approach is to quantize representations from a teacher network [6], [1]—however, these works focus solely on the RGB image domain. Not much work fo-

\*Equal contribution

cuses on unsupervised or self-supervised 3D object detection. Point cloud sparsity poses additional challenges, as the structure of data is significantly different from denser modalities.

The main body of state-of-the-art 3D object detection with point cloud literature comprises supervised learning methods [61, 54, 14, 36, 55, 37, 56, 39, 9, 21, 57]. Learning general point cloud representations is much more challenging than the denser RGB image domain.

Point cloud scene flow is another important 3D vision task. Initially, supervised learning was shown to be superior for the task [45, 25, 13, 51, 24, 50, 31]. More recently, self-supervised and unsupervised 3D scene flow and stereo flow methods have been introduced [48, 2, 18, 59, 63, 20, 7, 12, 33, 49, 27]. However, these developments have not been utilized for the 3D object detection task up until now.

We propose to employ a scene flow backbone trained in a self-supervised fashion to learn useful representations that other downstream head models can utilize after fine-tuning, such as a 3D object detection head (Fig. 1). First, we follow the cycle-consistency approach [29] to train a FlowNet3D-based [24] scene-flow backbone using self-supervised learning. We introduce architectural changes to the FlowNet3D module to incorporate a point cloud backbone that can also be utilized with a detection head. We explore several training and loss strategies, including auxiliary training, to find the best layout. Empirical evidence obtained from KITTI [11] and nuScenes [5] datasets show that the proposed strategy increases 3D detection performance significantly.

Our method differs from [29] in two important ways. To the best of our knowledge, lidar point cloud-based 3D object detection has not been successfully achieved with a self-supervised backbone up until now. Our modifications to the FlowNet3D [24] architecture enables the integration of temporal shift with 3D detection. Secondly, our combined auxiliary training cycle consistency and supervised 3D detection losses lead to learning more general representations as well as motion representations, which identify objects based on their contextual motion patterns.

A summary of our main contributions is as follows:

- Employing self-supervised point cloud scene flow estimation to learn motion representations for 3D object detection in tandem with supervised fine-tuning
- We show that auxiliary training is the best strategy for using self-supervised cycle-consistency loss along with supervised 3D detection loss.
- The proposed strategy is especially effective with a lesser amount of supervised data. We obtained a significant performance boost when only a smaller part of supervised training data was used for the 3D detection task.

## 2. Related Work

**Scene flow.** Scene flow was first introduced as an extension of optical flow in the third dimension and was estimated with a linear computation algorithm[41]. Stereo cameras [17, 42] and RGB-D were also [35] utilized to derive scene flow. Current state-of-the-art uses lidar point clouds and deep neural networks to estimate scene flow with supervised learning [24, 50, 13]. Most commonly, two subsequent lidar frames are used to estimate the flow vectors of each point in the scene. Building ground truth for such vectors is labor-intensive. As such, synthetic datasets are more popular for scene flow benchmarking [31].

**Self-supervised scene flow estimation.** Self-supervised scene flow estimation is a relatively understudied angle. A recently proposed solution [29] is to use cycle-consistency and nearest neighbors losses to train an estimation network. Several other distance metrics and regularization techniques such as using chamfer distance, smoothing, and regularization [52] have also been employed for the same task. A more recent study showed that self-supervised scene flow could be combined with motion segmentation also [3].

**Self-supervised 3D Object Detection.** A monocular 3D object detection model has been trained with self-supervised learning using shape priors, and 2D instance masks [4]. Another monocular 3D object detection model with weak supervision has been trained using shape priors [47]. [34] generates random synthetic point cloud scenes for pre-training to learn useful representations from CAD models. [53, 22, 16] mainly use contrastive pre-training to learn geometrical point cloud representations with different views of the same scene. However, there is not much work focusing on self-supervised 3D object detection considering motion representations with point clouds. We aim to fill this gap in the literature.

## 3. Method

Backbone of a 3D object detector is mainly used to extract point, voxel, or region features to detect possible objects in that vicinity. Due to the limitation in labelled dataset sizes, we aim to train the backbone on a large unlabelled dataset using self-supervision to obtain good motion-aware point representations. Afterwards, it is possible to use the pre-trained backbone for the 3D detection supervised training with a smaller dataset. Thus, the 3D detection network can benefit from the initialized point motion representations to distinguish objects based on movement patterns. We summarize our method in Fig. 2.

### 3.1. Problem Definition

Given two subsequent lidar point cloud frames  $\mathcal{P}_t = \{\mathbf{p}_i\}_M, \mathbf{p} \in \mathbb{R}^3$  and  $\mathcal{P}_{t+1} \in \mathbb{R}^{N \times 3}$ , we are first interested in estimating the scene flow  $\mathcal{F}_{t \rightarrow t+1} = \{d_i\}_M$ , where

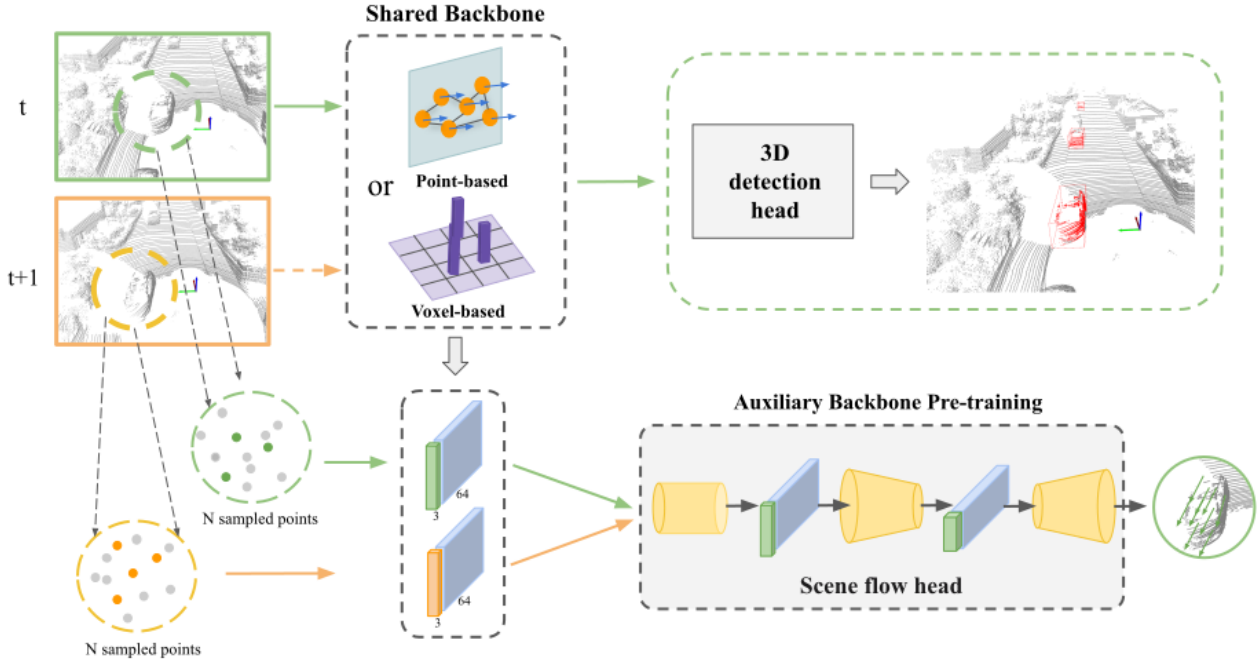


Figure 2: Our self-supervised 3D object detection pre-training: The auxiliary scene flow head is used to train the 3D detection backbone (point- or voxel-based) for motion-aware point cloud representations with self-supervised cycle consistency loss [29]. The motion representations learned without labelled data can help distinguish objects based on their motion patterns for a 3D downstream task. Then, we further train the pre-trained backbone and a 3D detection head for 3D detection with labelled data.

$\mathbf{d}_i = \mathbf{p}_i - \mathbf{p}'_i$ .  $\mathbf{p}'_i$  denotes the new position at time  $t + 1$  of point  $i$  in the first point cloud  $\mathcal{P}_t$ . It should be noted that the second point cloud may or may not contain a point corresponding to  $\mathbf{p}'_i$  due to sparsity. The second objective is to map  $\mathcal{P} \rightarrow \{T_j\}_U$ , where  $T_j$  is the 3D object detection tuple containing class id and bounding box shape and coordinates, using previously-learned spatio-temporal representations.  $U$  is the total number of objects in the point cloud frame.

We aim to benefit from the point motion representations learned by the 3D feature extractor,  $g$ , during self-supervised scene flow training  $\mathcal{F}_{t \rightarrow t+1} = s(g(\mathcal{P}_t, \mathcal{P}_{t+1}))$ , where  $s$  is the scene flow head. In this way, the 3D detection head,  $h$ , can use the spatio-temporal motion representations provided by  $g$  to better identify poor object point reflections for meaningful detection results such that  $\{T_j\}_U = h(g(\mathcal{P}))$ .

### 3.2. Self-supervised Scene Flow

**Backbone:** We first follow the cycle-consistency approach [29] to train a scene flow estimator. We use a 3D detector’s backbone to extract local features of sam-

pled points from two consecutive frames. This allows the self-supervised scene flow gradients to be backpropagated through the backbone. Hence, the backbone learns point representations encoding object movement patterns. The learned spatio-temporal features can be further used to distinguish objects from the background and other objects for the 3D perception task.

**Scene Flow Head:** The scene flow head based on FlowNet3D [24] generates flow embeddings from local point features provided by the 3D backbone. The shape of input points,  $\mathcal{P}_t$ , is reconstructed by applying *set upconv layers* to local flow embeddings for the final scene flow estimations  $\mathcal{F}_{t \rightarrow t+1}$ .

**Training with Cycle Consistency:** We use 3D detection backbone as the feature extractor for the scene flow head. Both the backbone and the scene flow head are trained with the self-supervised cycle consistency loss given in [29]. For the cycle consistency, the scene flow is calculated in forward and backward directions, meaning  $\mathcal{F}_{t \rightarrow t+1}$  and  $\mathcal{F}_{t+1 \rightarrow t}$ . The  $\mathcal{F}_{t+1 \rightarrow t}$  makes use of the new positions of the propagated points  $\mathbf{p}'_i$  to close the cycle. The  $\mathbf{p}''_i$  is the estimated positions of the  $\mathbf{p}_i$  in the backward direction with

the  $\mathcal{F}_{t+1 \rightarrow t}$ . The mismatch between the  $\mathbf{p}_i$  and the  $\mathbf{p}_i''$  at frame  $t$  allows training of the backbone in a self-supervised way. With the self-supervised training, 3D backbone learns to generate regional flow and motion features from the given set of point clouds.

### 3.3. Downstream Task: 3D Object Detection

We are interested in the 3D object detection as the 3D downstream task. The scene flow head,  $s$ , and the 3D object detection head,  $h$ , use the same backbone,  $g$ , as seen in Fig. 2. Also, point- or voxel-based 3D backbone encodings can be used. We initialize 3D detector’s backbone weights with the pre-trained weights from the self-supervised scene flow training. In this way, we assume that the pre-trained backbone from scene flow can already provide good geometry- and motion-aware point features. The 3D detection head takes distinguishable spatio-temporal point cloud features based on different object motion patterns. Hence, the 3D detection network can detect objects more accurately even after supervised training with a smaller labelled dataset. We show the efficacy of our approach in section 5. Note that the scene flow head is for the auxiliary scene flow training and is not used during the 3D detection training and inference.

## 4. Implementation Details

Our self-supervised backbone pre-training approach can be used with different 3D detector architectures. We evaluate our method with mainly two different 3D detectors, Point-GNN<sup>1</sup> [39] and PointPillars<sup>2</sup> [21], which are point- and voxel-based approaches, respectively. For the self-supervised scene flow task, we add the modified FlowNet3D as well as the cycle-consistency loss<sup>3</sup> to 3D detectors’ training pipelines.

### 4.1. Pre-training with Self-supervised Scene Flow

The FlowNet3D takes a set of points from two successive frames as input and estimates the flow vectors. The network extracts the point features with two cascaded *PointNet Set Abstraction* modules, each with a 3-layer MLP. We remove the first *PointNet Set Abstraction* module and feed in the point features from 3D detector’s backbone to the second *PointNet Set Abstraction* module.

**Point cloud backbone:** We use Point-GNN and PointPillars backbones for our main results and CenterPoint backbone for the ablation, which has the same architecture with PointPillars backbone. Point-GNN extracts keypoint features from a 3-level graph network used as a backbone, from which we obtain keypoint features of two consecutive point clouds. After sampling  $N$  points from each frame, we

<sup>1</sup><https://github.com/WeijingShi/Point-GNN>

<sup>2</sup><https://github.com/open-mmlab/mmdetection3d/>

<sup>3</sup><https://github.com/HimangiM/Just-Go-with-the-Flow-Self-Supervised-Scene-Flow-Estimation>

apply bilinear interpolation to get features of the sampled points from keypoint features according to their positions. We use the settings provided for the best performing Point-GNN with  $T = 3$ . For the PointPillars detector, we follow a similar approach and use its voxel encoder to obtain features of the sampled points from two consecutive frames without making any changes to the 3D detector’s architecture.

**Scene flow head:** Scene flow head is responsible for estimating 3D motion of the points between two sequential frames. The FlowNet3D’s scene flow head consists of *flow embedding*, *set conv layers*, and *set upconv layers* followed by fully-connected layers for estimating point flow vectors. The scene flow head takes the local point features as inputs. We remove only the final *set upconv layer* that takes skip connections from the first *PointNet Set Abstraction* module, which we replace with 3D detector’s backbone.

**Training strategy:** We train the point cloud backbone and scene flow head end-to-end using the self-supervised scene flow loss. As a common practise, we initialize our scene flow head weights with the pre-trained FlowNet3D weights on the supervised FlyingThings3D [28] simulation data. For the scene flow training on Point-GNN backbone, we use Stochastic Gradient Descent (SGD) optimizer with  $6.25 \times 10^{-5}$  learning rate. The number of sampled points from each frame is  $N = 2048$ . We train the scene flow network for 80k steps on the KITTI tracking dataset without using any labels. The model is trained on a single Nvidia Tesla V100 GPU. For the PointPillars-based scene flow training, we use AdamW optimizer using the voxel encoders as the backbone with a 0.001 learning rate. Our batch size is 2 for  $N = 2048$  sampled points. We trained the network for 4 epochs on one Nvidia RTX 3090 GPU. For the scene flow training on CenterPoint[58], our settings are the same as the PointPillars scene flow training settings.

### 4.2. 3D Detection Fine-tuning

**3D detection heads:** We use Point-GNN and PointPillars as the 3D detectors for our main results and CenterPoint for ablation study results to show the efficacy of our self-supervised scene flow pre-training approach. We initialize detectors’ backbone weights with the pre-trained backbone weights from the scene flow task for a better point feature representation.

**Training strategy:** After initializing weights of the 3D detector backbone from the scene flow task, we further train the backbone and the 3D detection heads with the 3D detection loss. We apply an alternating training strategy between the self-supervised scene flow and supervised 3D detection trainings: **(i)** Train the backbone and the scene flow head for self-supervised scene flow, **(ii)** train the pre-trained backbone and the detection head with 3D detection training, **(iii)** train the backbone from step (ii) and the scene flow head from step (i) for the scene flow, and finally **(iv)** train the

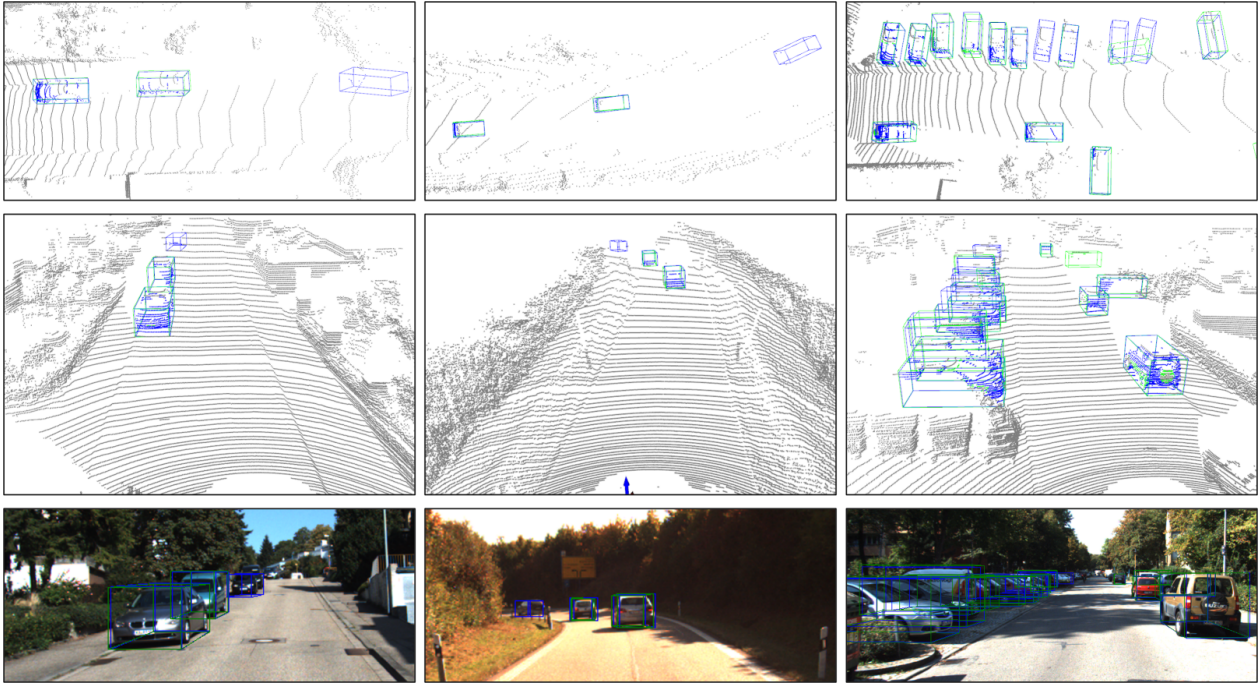


Figure 3: Qualitative Results: Three different scenes from the KITTI 3D Detection validation set in the columns. Blue and green bounding boxes are for our approach and the baseline Point-GNN [39], respectively. In the left-most column, our method is able to detect a distant hard object while the baseline misses it. Similarly, our self-supervised Point-GNN can detect the moving distant car unlike the baseline (middle column) and performs better in a denser environment (right-most column).

backbone from step (iii) and the detection head from step (ii) for 3D detection.

We train the Point-GNN baseline for  $1400k$  steps using the SGD optimizer with a learning rate of 0.125 as suggested by Point-GNN’s authors [39]. For the training in step (ii) and step (iv), we use SGD with a learning rate of 0.1. The trainings took place on an Nvidia Tesla V100 GPU. We use batch size 4 for all Point-GNN trainings. The PointPillars detector is trained for 24 epochs with a batch size of 4 and a learning rate of 0.001 using AdamW optimizer. We used two Nvidia RTX 2080 Ti GPUs for the training. For the CenterPoint, we used AdamW as the optimizer with a learning rate  $1e - 4$ . The model was trained for 20 epochs with a batch size of 20 on one Nvidia RTX 3090 GPU.

### 4.3. Datasets

We use KITTI 3D Object Detection, KITTI Multi-object Tracking datasets [11] as well as nuScenes dataset [5] for the self-supervised scene flow and the supervised 3D detection training and validation.

**KITTI 3D Object Detection:** KITTI 3D Object Detection dataset consists of 7481 training frames sampled from different drives. Since the provided frames are not sequential, we use lidar point clouds only for 3D object detection

training. Only objects visible in the camera-view are annotated. We utilize the common train-val split with 3712 training and 3769 validation samples. For the evaluation, the KITTI average precision (AP) metric is used for three different difficulty levels with  $IoU = 0.7$  for the car class.

**KITTI Multi-object Tracking:** This dataset contains 21 training and 29 testing drives, each of which consists of several sequential frames. We use the tracking dataset only for the self-supervised scene flow training without using any annotations. Therefore, we combine all the training and testing drive data for training except the training drives 11, 15, 16, and 18, which are used for observing cycle consistency validation loss. This gives us 11902 frames for self-supervised scene flow training.

**nuScenes:** nuScenes is also an autonomous driving dataset, which consists of 700 training and 150 validation drives. The annotations are provided at 2 Hz for 360-degree objects and the lidar sweeps are collected at 20 Hz. nuScenes is a larger dataset than KITTI and it is collected from denser and more challenging environments. There are 10 classes annotated in the nuScenes dataset. The main metrics are the average precision (AP) per class, mean average precision (mAP) among all classes, and the nuScenes detection score (NDS). Since the provided data contains se-

Method	Car (IoU=0.7)			3D AP			BEV AP		
	Easy	Mod	Hard	Easy	Mod	Hard			
Point-GNN* [39]	90.44	82.12	77.70	93.03	89.31	86.86			
<b>Self-supervised Point-GNN</b>	<b>91.43</b>	<b>82.85</b>	<b>80.12</b>	<b>93.55</b>	<b>89.79</b>	<b>87.23</b>			
Improvement	<b>+0.99</b>	<b>+0.73</b>	<b>+2.42</b>	<b>+0.52</b>	<b>+0.48</b>	<b>+0.37</b>			

Table 1: Self-supervised Point-GNN compared with the baseline on KITTI val. set for car class using 3D AP<sub>R<sub>40</sub></sub> metric. (\*Reproduced baseline results for AP<sub>R<sub>40</sub></sub>.)

quential lidar point clouds, we use this dataset for both self-supervised scene flow and 3D detection trainings.

#### 4.4. Loss

For the 3D object detection training, we keep the same loss functions used for the 3D detectors.

**Point-GNN[39]:** Point-GNN combines localization, classification, and regularization losses. Classification loss is calculated with the average cross-entropy loss among four classes, which are *background*, horizontal and vertical anchor box classes, and a *don't care* class. The network regresses 7 bounding box parameters,  $(x, y, z)$  for the center coordinates,  $(w, h, l)$  for the width, height, and length sizes, and  $\theta$  for the orientation of the bounding box. The Huber loss and  $L1$  regularization are used as regression and regularization losses, respectively. We use the original loss coefficients for the total loss.

**PointPillars[21]:** Similarly, PointPillars regresses the 7 bounding box parameters and utilizes the Huber loss as a regression loss. The orientation is predicted from a set of discrete bins, for which the softmax classification loss is utilized. The focal loss is used as a classification loss for the object classes. All the loss values are combined with respective coefficients for the total loss and we use the default values given in the *mmetection3d* repository.

**Self-supervised scene flow loss:** We utilize the self-supervised loss used in [29] for training the 3D detector backbone and the scene flow head. The loss consists of the nearest neighbor and the cycle consistency losses. The nearest neighbor loss calculates the Euclidean distance of the point  $\mathbf{p}'_i$  to its nearest neighbor in frame  $t + 1$ .  $\mathbf{p}'_i$  is the point transformed from frame  $t$  to  $t + 1$ . For the cycle consistency loss calculation the flow is applied in the forward ( $\mathcal{F}_{t \rightarrow t+1}$ ) and the backward ( $\mathcal{F}_{t+1 \rightarrow t}$ ) directions. The distance between the resulting  $\mathbf{p}''_i$  point and its anchor  $\mathbf{p}_i$  is used for the cycle consistency loss. Both losses are summed up for the total loss and only this loss is used for the training of the backbone and the scene flow head.

#### 4.5. Experiments

We conduct several experiments to show the efficacy of our self-supervised pre-training method on 3D object detection task using Point-GNN, PointPillars, and CenterPoint

Method	Car (IoU=0.7)			3D AP		
	Easy	Mod	Hard	Easy	Mod	Hard
VoxelNet[61]	81.97	65.46	62.85			
F-PointNet[32]	83.76	70.92	63.65			
AVOD[19]	84.41	74.44	68.65			
SECOND[54]	87.43	76.48	69.10			
PointPillars[21]	-	77.98	-			
Point-GNN [39]	87.89	78.34	77.38			
<b>Self-supervised Point-GNN</b>	<b>88.32</b>	<b>78.66</b>	<b>77.92</b>			

Table 2: Self-supervised Point-GNN 3D AP<sub>R<sub>11</sub></sub> car results on KITTI validation set.

3D detectors. For our main results, we compare the self-supervised Point-GNN with the baseline on KITTI 3D object detection dataset test and validation splits. We conduct a similar experiment using the PointPillars detector on the nuScenes test and validation sets as well as the KITTI validation set.

In addition to our main 3D detection results, we conduct further experiments to investigate how much detection gain is obtained using our self-supervised scene flow pre-training with limited annotated 3D detection training data. For these experiments, we train the self-supervised 3D detectors (Point-GNN, PointPillars, and CenterPoint) and their baselines with a percentage of the annotated KITTI and nuScenes 3D detection data. Moreover, we compare detection accuracy of self-supervised Point-GNN trained with and without alternating training strategy to justify our alternating self-supervised scene flow and supervised 3D detection scheme.

## 5. Results & Discussion

In this section, we provide our main results obtained using our scene flow-based self-supervised training with Point-GNN and PointPillars 3D detectors on KITTI and nuScenes validation and test sets.

### 5.1. Point-GNN

We present our self-supervised scene flow pre-training results with Point-GNN 3D detector in Tables 1, 2, and 4. The self-supervised Point-GNN is pre-trained on the

Method	mAP	NDS	Car	Ped	Bus	Barrier	T. C.	Truck	Trailer	Moto.
SECOND[54]	27.12	-	75.53	59.86	29.04	32.21	22.49	21.88	12.96	16.89
PointPillars*[21]	40.02	53.29	80.60	72.40	46.30	52.60	33.60	35.10	26.20	38.40
<b>Self-supervised PointPillars</b>	<b>42.06</b>	<b>55.02</b>	<b>81.10</b>	<b>74.50</b>	<b>49.50</b>	<b>54.70</b>	<b>34.70</b>	<b>38.40</b>	<b>29.70</b>	<b>38.80</b>
CenterPoint*[58]	49.13	59.73	83.70	77.40	<b>61.90</b>	59.40	<b>52.90</b>	50.20	35.00	<b>44.40</b>
<b>Self-supervised CenterPoint</b>	<b>49.89</b>	<b>60.01</b>	<b>84.10</b>	<b>77.90</b>	61.50	<b>61.00</b>	<b>52.50</b>	<b>51.00</b>	<b>35.20</b>	44.10

Table 3: Self-supervised PointPillars and CenterPoint results on nuScenes validation set. (\* mm detection3d PointPillars and CenterPoint checkpoint results, on which we built our work.)

scene flow task with cycle consistency loss using KITTI Tracking dataset without any annotations. Following, it is trained with the annotated KITTI 3D detection dataset using the proposed alternating training scheme. The baseline is trained using the same configuration and hyper-parameters. The only difference is that the baseline network weights are initialized randomly. Table 1 shows the 3D and BEV AP<sub>R<sub>40</sub></sub> scores of the baseline and self-supervised Point-GNN, where our method outperforms the baseline in all difficulty levels and especially with a large margin in hard difficulty level ( 2.5%). This shows that motion-related point representations help distinguish even difficult objects that reflect only a small number of points.

Point-GNN paper [38] provides its KITTI validation set scores with AP<sub>R<sub>11</sub></sub> metric. Therefore, we show the same comparison using the AP<sub>R<sub>11</sub></sub> in Table 2 with the baseline as well as the previous state-of-the-art. The baseline Point-GNN AP<sub>R<sub>11</sub></sub> scores are taken from the Point-GNN paper [39]. Similarly, our self-supervised Point-GNN outperforms the baseline on all difficulty levels.

Finally, we compare our self-supervised Point-GNN with the baseline Point-GNN as well as with the previous state-of-the-art on the KITTI test set as the results given in Table 4. Consistently, we enhance the baseline detection accuracy in the hard level with a 2% increase. The Fig. 3 shows our qualitative results on KITTI 3D Object Detection scenes. The blue bounding boxes and green bounding boxes indicate results of our approach and the baseline, respectively. We show the bird’s eye view and front-view lidar visualizations at the top and middle rows. At the bottom, we show the projected 3D bounding boxes on the image plane. Our approach can detect distant objects (left-most column) better as well as distant and moving objects (middle column). In addition, as seen in the right-most column of Fig. 3, our approach can provide better detection results in a denser scene.

## 5.2. PointPillars

We also report results of our self-supervised pre-training method using PointPillars [21] 3D detector on the nuScenes

Method	Car (IoU=0.7)			3D AP		
	Easy	Mod	Hard	Easy	Mod	Hard
AVOD[19]	76.39	66.47	60.23			
F-PointNet[32]	82.19	69.79	60.59			
TANet[26]	84.39	75.94	68.82			
Associate-3Ddet[10]	85.99	77.40	70.53			
UBER-ATG-MMF[23]	88.40	77.43	70.22			
CenterNet3D[44]	86.20	77.90	73.03			
SECOND[54]	87.44	79.46	73.97			
SERCNN[60]	87.74	78.96	74.30			
Point-GNN [39]	88.33	79.47	72.29			
<b>Self-supervised Point-GNN</b>	87.78	79.36	74.15			

Table 4: Self-supervised Point-GNN KITTI Test results: 3D AP<sub>R<sub>40</sub></sub> on Car class.

and KITTI datasets. We pre-train the PointPillars voxel encoder with the self-supervised scene flow task without annotations. Following, the entire PointPillars network is trained on the annotated 3D detection data using our alternating training strategy. In Table 3, we compare our self-supervised PointPillars with the baseline on nuScenes validation set. The baseline results are obtained from the best checkpoint given in the well-known mm detection3d repository [8]. Our self-supervised PointPillars outperforms the baseline with a large increment on mAP and NDS metrics ( 2%) as well as for all class scores. Moreover, we provide results of our self-supervised PointPillars on nuScenes test set in Table 5 comparing to the previously-submitted PointPillars versions from the nuScenes leaderboard.

We compare our self-supervised PointPillars with the baseline on the KITTI validation set as given in Table 6. Consistent with the previously-introduced results, our method improves the baseline results with a large margin for the 3D detection task. The increment is the most obvious for moderate and hard difficulty levels with 2.3% and 6.5%, respectively.

Method	mAP	NDS	Car	Ped	Bus	Barrier	T. C.	Truck	Trailer	Moto.
PointPillars[21]	30.50	45.30	68.40	59.70	28.20	38.90	30.80	23.00	23.40	27.40
InfoFocus[46]	39.50	39.50	77.90	63.40	44.80	47.80	46.50	31.40	37.30	29.00
PointPillars+[43]	40.10	55.00	76.00	64.00	32.10	56.40	45.60	31.00	36.60	34.20
<b>Self-supervised PointPillars</b>	43.63	56.28	81.00	73.10	37.10	58.20	47.80	36.10	41.80	35.40
<b>Self-supervised CenterPoint*</b>	51.42	60.92	83.80	77.00	56.80	65.10	63.90	46.30	48.50	41.10

Table 5: Self-supervised PointPillars result on nuScenes test set comparing with other PointPillars-based submissions from the nuScenes leaderboard. (\* CenterPoint test results obtained with the same training hyperparameters as the CenterPoint used for validation scores, which is different from the original CenterPoint [58] to fit in available GPUs. )

Method	Car (IoU=0.7)			3D AP			BEV AP		
	Easy	Mod	Hard	Easy	Mod	Hard	Easy	Mod	Hard
PointPillars [21]	85.41	73.98	67.76	89.93	86.57	85.20			
<b>Self-supervised PointPillars</b>	<b>85.92</b>	<b>76.33</b>	<b>74.32</b>	<b>89.96</b>	<b>87.44</b>	<b>85.53</b>			
Improvement	+0.51	+2.36	+6.56	+0.03	+0.87	+0.33			

Table 6: Self-supervised PointPillars 3D AP<sub>R<sub>40</sub></sub> results on KITTI validation set for the car class.

### 5.3. CenterPoint

In addition to the Point-GNN and PointPillars results, we trained the CenterPoint [58] detector with our self-supervised pre-training scheme to further evaluate the usefulness of our method. Table 3 compares our self-supervised CenterPoint with its baseline, which we obtained from the provided mmdetection3d [8] checkpoint. Compared to the available checkpoint, our self-supervised scene flow pre-training method enhances the 3D detection scores on nuScenes dataset for mAP and NDS metrics as well as for almost all classes. We note that the CenterPoint is a state-of-the-art 3D detector with a heavy and optimized training schedule. Therefore, we needed to adapt its hyperparameters given with mmdetection3d to fit in our GPUs as explained in 4.2. We think that this caused a sub-optimal CenterPoint training. Nevertheless, our self-supervised CenterPoint outperforms the optimized baseline. We also provide our test scores on nuScenes dataset in Table 5. We obtained the test scores with the same training settings as the self-supervised CenterPoint used for validation, which are suboptimal compared to the original CenterPoint training due to the hardware limitations.

### 5.4. Ablation Study

We conduct two types of ablation studies to further justify the effectiveness of our self-supervised pre-training approach: (i) performance after training with limited annotated data and (ii) performance with and without alternating training strategy. Datasets with 3D annotations are mostly limited for the real-world scenarios due to expense and difficulty of requiring expert knowledge for the annotation pro-

cess. To show our method’s enhancement over the baseline using the self-supervised pre-training, we train our self-supervised 3D detectors and baselines with a percentage of the annotated datasets.

In Table 7, we show the performance of self-supervised Point-GNN and the baseline trained with 1%, 5%, and 20% of the KITTI train split. Our method consistently outperforms the baseline for all difficulty levels on KITTI validation set. We note that all self-supervised 3D detector ablation results are obtained without alternating training except the alternating training ablation. Table 8 presents results of the same experiments with the PointPillars detector trained on 2.5%, 5%, and 10% of the nuScenes train splits. Self-supervised PointPillars similarly outperforms the baseline for mAP and AP for car and pedestrian classes. We conduct the same experiment with the CenterPoint 3D detector as the results are given in Table 9. We also observe an obvious increase in the 3D detection mAP scores with our self-supervised CenterPoint detector. Further, the effect of the alternating training strategy is shown in B. Overall, the results suggest that the self-supervised scene flow pre-training can help learn more representative point-wise features in the lack of labelled training data.

In addition, we conduct an ablation study to justify our alternating training strategy. The alternating training enhances the hard difficulty 3D AP with 2.32% increment. We think that this improvement is due to the repeated motion-awareness of the backbone brought by the first 3D detection fine-tuning. The detailed 3D and BEV AP results are provided in the supplementary material.

Fig. 4 shows visualized sparse scene flow estimations on the sampled KITTI lidar point clouds obtained using Point-

Training Data Size	1%			5%			20%		
	Easy	Mod	Hard	Easy	Mod	Hard	Easy	Mod	Hard
Car AP (IoU=0.7)	63.34	50.92	44.05	81.26	71.27	65.05	88.47	77.20	74.20
<b>SSL Point-GNN</b>	<b>66.47</b>	<b>51.42</b>	<b>44.63</b>	<b>84.04</b>	<b>72.69</b>	<b>65.93</b>	<b>88.65</b>	<b>79.52</b>	<b>74.87</b>
Improvement	<b>+3.13</b>	<b>+0.50</b>	<b>+0.58</b>	<b>+2.78</b>	<b>+1.42</b>	<b>+0.88</b>	<b>+0.18</b>	<b>+2.32</b>	<b>+0.67</b>

Table 7: Self-supervised (SSL) Point-GNN trained with a percentage (1%, 5%, and 20%) of labelled 3D detection data. 3D AP<sub>R<sub>40</sub></sub> results for car class on KITTI val. set.

Training Data Size	2.5%			5%			10%		
	mAP	Car	Ped	mAP	Car	Ped	mAP	Car	Ped
PointPillars	2.99	24.60	10.30	10.93	52.30	29.00	13.02	55.50	32.20
<b>SSL PointPillars</b>	<b>4.57</b>	<b>30.10</b>	<b>10.70</b>	<b>11.12</b>	<b>53.30</b>	<b>29.20</b>	<b>13.36</b>	<b>56.80</b>	<b>33.60</b>

Table 8: Self-supervised (SSL) PointPillars results on the nuScenes validation set. Both the baseline and self-supervised PointPillars are trained only with 2.5%, 5%, and 10% of the nuScenes training split.

nuScenes Validation Set	mAP			
	1%	2.5%	5%	10%
Training Data Size	13.56	27.04	34.28	41.29
<b>SSL CenterPoint</b>	<b>14.88</b>	<b>28.10</b>	<b>35.46</b>	<b>41.88</b>

Table 9: Self-supervised (SSL) CenterPoint 3D detection mAP scores on nuScenes validation set trained with a smaller amount of labelled data.

GNN backbone. Red points are the sparsely-sampled points at frame  $t$ , which are propagated to the frame  $t + 1$  using the estimated flow vectors as shown with the green points. The green points closely match the gray points, which are the original point cloud at frame  $t + 1$ . The network is trained with the cycle consistency loss followed by a 100 epoch fine-tuning on the KITTI Scene Flow Dataset following [29]. This suggests that our scene flow network learns useful point features and therefore the point cloud motion patterns, which improves the 3D object detection accuracy.

## 6. Conclusion

In this study, we propose a self-supervised backbone training approach for 3D object detection method. We utilize large unlabelled datasets for self-supervised training of the 3D detection backbone. The scene flow task is used for the self-supervision using the cycle consistency, which helps the backbone learning the point cloud data structure. We show that our approach can improve the detection results of different 3D detectors comparing to their baselines on KITTI and nuScenes datasets. We also show that self-supervised pre-training is especially helpful with the lack of data. Our approach is flexible and can be combined with different point- and voxel-based 3D detectors.

## References

- [1] Yuki Markus Asano, Christian Rupprecht, and Andrea Vedaldi. Self-labelling via simultaneous clustering and representation learning. *arXiv preprint arXiv:1911.05371*, 2019. [1](#)
- [2] Tali Basha, Yael Moses, and Nahum Kiryati. Multi-view scene flow estimation: A view centered variational approach. *International journal of computer vision*, 101(1):6–21, 2013. [2](#)
- [3] Stefan Andreas Baur, David Josef Emmerichs, Frank Moosmann, Peter Pinggera, Bjorn Ommer, and Andreas Geiger. Slim: Self-supervised lidar scene flow and motion segmentation. In *Proceedings of the IEEE/CVF International Conference on Computer Vision*, pages 13126–13136, 2021. [2](#)
- [4] Deniz Beker, Hiroharu Kato, Mihai Adrian Morariu, Takahiro Ando, Toru Matsuoka, Wadim Kehl, and Adrien Gaidon. Monocular differentiable rendering for self-supervised 3d object detection. In *Computer Vision–ECCV 2020: 16th European Conference, Glasgow, UK, August 23–28, 2020, Proceedings, Part XXI 16*, pages 514–529. Springer, 2020. [2](#)
- [5] Holger Caesar, Varun Bankiti, Alex H Lang, Sourabh Vora, Venice Erin Liong, Qiang Xu, Anush Krishnan, Yu Pan, Giacomo Baldan, and Oscar Beijbom. nuscenes: A multimodal dataset for autonomous driving. In *Proceedings of the IEEE/CVF conference on computer vision and pattern recognition*, pages 11621–11631, 2020. [2, 5](#)
- [6] Mathilde Caron, Ishan Misra, Julien Mairal, Priya Goyal, Piotr Bojanowski, and Armand Joulin. Unsupervised learning of visual features by contrasting cluster assignments. *arXiv preprint arXiv:2006.09882*, 2020. [1](#)
- [7] Yuhua Chen, Cordelia Schmid, and Cristian Sminchisescu. Self-supervised learning with geometric constraints in monocular video: Connecting flow, depth, and camera. In *Proceedings of the IEEE/CVF International Conference on Computer Vision*, pages 7063–7072, 2019. [2](#)
- [8] MMDetection3D Contributors. MMDetection3D: Open-MMLab next-generation platform for general 3D object

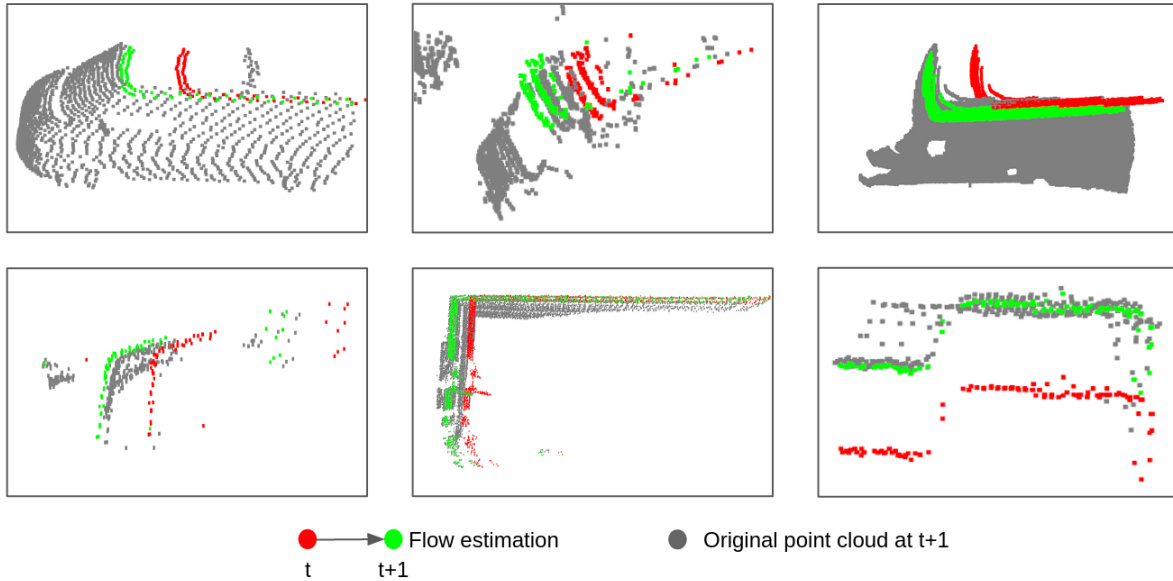


Figure 4: Sparse scene flow estimation on the sampled KITTI lidar points from different frames. Gray points are from the full point clouds at frame  $t + 1$ , red points are sampled points at frame  $t$ , and green ones are the propagated points to the frame  $t + 1$  using scene flow estimation.

detection. <https://github.com/open-mmlab/mmdetection3d>, 2020. 7, 8

[9] Jiajun Deng, Shaoshuai Shi, Peiwei Li, Wengang Zhou, Yanyong Zhang, and Houqiang Li. Voxel r-cnn: Towards high performance voxel-based 3d object detection. In *Proceedings of the AAAI Conference on Artificial Intelligence*, volume 35, pages 1201–1209, 2021. 2

[10] Liang Du, Xiaoqing Ye, Xiao Tan, Jianfeng Feng, Zhenbo Xu, Errui Ding, and Shilei Wen. Associate-3ddet: Perceptual-to-conceptual association for 3d point cloud object detection. In *Proceedings of the IEEE/CVF conference on computer vision and pattern recognition*, pages 13329–13338, 2020. 7

[11] Andreas Geiger, Philip Lenz, and Raquel Urtasun. Are we ready for autonomous driving? the kitti vision benchmark suite. In *2012 IEEE conference on computer vision and pattern recognition*, pages 3354–3361. IEEE, 2012. 2, 5

[12] Clément Godard, Oisin Mac Aodha, Michael Firman, and Gabriel J Brostow. Digging into self-supervised monocular depth estimation. In *Proceedings of the IEEE/CVF International Conference on Computer Vision*, pages 3828–3838, 2019. 2

[13] Xiuye Gu, Yijie Wang, Chongruo Wu, Yong Jae Lee, and Panqu Wang. Hplflownet: Hierarchical permutohedral lattice flownet for scene flow estimation on large-scale point clouds. In *Proceedings of the IEEE/CVF Conference on Computer Vision and Pattern Recognition*, pages 3254–3263, 2019. 2

[14] Chenhang He, Hui Zeng, Jianqiang Huang, Xian-Sheng Hua, and Lei Zhang. Structure aware single-stage 3d object detection from point cloud. In *Proceedings of the IEEE/CVF Conference on Computer Vision and Pattern Recognition*, pages 11873–11882, 2020. 2

[15] Kaiming He, Haoqi Fan, Yuxin Wu, Saining Xie, and Ross Girshick. Momentum contrast for unsupervised visual representation learning. In *Proceedings of the IEEE/CVF Conference on Computer Vision and Pattern Recognition*, pages 9729–9738, 2020. 1

[16] Ji Hou, Benjamin Graham, Matthias Nießner, and Saining Xie. Exploring data-efficient 3d scene understanding with contrastive scene contexts. In *Proceedings of the IEEE/CVF Conference on Computer Vision and Pattern Recognition*, pages 15587–15597, 2021. 2

[17] Frédéric Huguet and Frédéric Devernay. A variational method for scene flow estimation from stereo sequences. In *2007 IEEE 11th International Conference on Computer Vision*, pages 1–7. IEEE, 2007. 2

[18] Junhwa Hur and Stefan Roth. Self-supervised monocular scene flow estimation. In *Proceedings of the IEEE/CVF Conference on Computer Vision and Pattern Recognition*, pages 7396–7405, 2020. 2

[19] Jason Ku, Melissa Mozifian, Jungwook Lee, Ali Harakeh, and Steven L Waslander. Joint 3d proposal generation and object detection from view aggregation. In *2018 IEEE/RSJ International Conference on Intelligent Robots and Systems (IROS)*, pages 1–8. IEEE, 2018. 6, 7

[20] Hsueh-Ying Lai, Yi-Hsuan Tsai, and Wei-Chen Chiu. Bridging stereo matching and optical flow via spatiotemporal correspondence. In *Proceedings of the IEEE/CVF Conference on Computer Vision and Pattern Recognition*, pages 1890–1899, 2019. 2

[21] Alex H Lang, Sourabh Vora, Holger Caesar, Lubing Zhou, Jiong Yang, and Oscar Beijbom. Pointpillars: Fast encoders for object detection from point clouds. In *Proceedings of the IEEE/CVF Conference on Computer Vision and Pattern Recognition*, pages 1890–1899, 2019. 2

*the IEEE/CVF Conference on Computer Vision and Pattern Recognition*, pages 12697–12705, 2019. 2, 4, 6, 7, 8, 13, 14

[22] Hanxue Liang, Chenhan Jiang, Dapeng Feng, Xin Chen, Hang Xu, Xiaodan Liang, Wei Zhang, Zhenguo Li, and Luc Van Gool. Exploring geometry-aware contrast and clustering harmonization for self-supervised 3d object detection. In *Proceedings of the IEEE/CVF International Conference on Computer Vision*, pages 3293–3302, 2021. 2

[23] Ming Liang, Bin Yang, Yun Chen, Rui Hu, and Raquel Urtasun. Multi-task multi-sensor fusion for 3d object detection. In *Proceedings of the IEEE/CVF Conference on Computer Vision and Pattern Recognition*, pages 7345–7353, 2019. 7

[24] Xingyu Liu, Charles R Qi, and Leonidas J Guibas. Flownet3d: Learning scene flow in 3d point clouds. In *Proceedings of the IEEE/CVF Conference on Computer Vision and Pattern Recognition*, pages 529–537, 2019. 2, 3

[25] Xingyu Liu, Mengyuan Yan, and Jeannette Bohg. Meteoronet: Deep learning on dynamic 3d point cloud sequences. In *Proceedings of the IEEE/CVF International Conference on Computer Vision*, pages 9246–9255, 2019. 2

[26] Zhe Liu, Xin Zhao, Tengteng Huang, Ruolan Hu, Yu Zhou, and Xiang Bai. Tanet: Robust 3d object detection from point clouds with triple attention. In *Proceedings of the AAAI Conference on Artificial Intelligence*, volume 34, pages 11677–11684, 2020. 7

[27] Chenxu Luo, Zhenheng Yang, Peng Wang, Yang Wang, Wei Xu, Ram Nevatia, and Alan Yuille. Every pixel counts++: Joint learning of geometry and motion with 3d holistic understanding. *IEEE transactions on pattern analysis and machine intelligence*, 42(10):2624–2641, 2019. 2

[28] Nikolaus Mayer, Eddy Ilg, Philip Hausser, Philipp Fischer, Daniel Cremers, Alexey Dosovitskiy, and Thomas Brox. A large dataset to train convolutional networks for disparity, optical flow, and scene flow estimation. In *Proceedings of the IEEE conference on computer vision and pattern recognition*, pages 4040–4048, 2016. 4

[29] Himangi Mittal, Brian Okorn, and David Held. Just go with the flow: Self-supervised scene flow estimation. In *Proceedings of the IEEE/CVF Conference on Computer Vision and Pattern Recognition*, pages 11177–11185, 2020. 2, 3, 6, 9

[30] Senthil Purushwalkam Shiva Prakash and Abhinav Gupta. Demystifying contrastive self-supervised learning: Invariances, augmentations and dataset biases. *Advances in Neural Information Processing Systems*, 33, 2020. 1

[31] Gilles Puy, Alexandre Boulch, and Renaud Marlet. Flot: Scene flow on point clouds guided by optimal transport. In *Computer Vision–ECCV 2020: 16th European Conference, Glasgow, UK, August 23–28, 2020, Proceedings, Part XXVIII 16*, pages 527–544. Springer, 2020. 2

[32] Charles R Qi, Wei Liu, Chenxia Wu, Hao Su, and Leonidas J Guibas. Frustum pointnets for 3d object detection from rgbd data. In *Proceedings of the IEEE conference on computer vision and pattern recognition*, pages 918–927, 2018. 6, 7

[33] Anurag Ranjan, Varun Jampani, Lukas Balles, Kihwan Kim, Deqing Sun, Jonas Wulff, and Michael J Black. Competitive collaboration: Joint unsupervised learning of depth, camera motion, optical flow and motion segmentation. In *Proceedings of the IEEE/CVF Conference on Computer Vision and Pattern Recognition*, pages 12240–12249, 2019. 2

[34] Yongming Rao, Benlin Liu, Yi Wei, Jiwen Lu, Cho-Jui Hsieh, and Jie Zhou. Randomrooms: Unsupervised pre-training from synthetic shapes and randomized layouts for 3d object detection. In *Proceedings of the IEEE/CVF International Conference on Computer Vision*, pages 3283–3292, 2021. 2

[35] Lin Shao, Parth Shah, Vikranth Dwaracherla, and Jeannette Bohg. Motion-based object segmentation based on dense rgbd scene flow. *IEEE Robotics and Automation Letters*, 3(4):3797–3804, 2018. 2

[36] Shaoshuai Shi, Chaoxu Guo, Li Jiang, Zhe Wang, Jianping Shi, Xiaogang Wang, and Hongsheng Li. Pv-rcnn: Point-voxel feature set abstraction for 3d object detection. In *Proceedings of the IEEE/CVF Conference on Computer Vision and Pattern Recognition*, pages 10529–10538, 2020. 2

[37] Shaoshuai Shi, Xiaogang Wang, and Hongsheng Li. Pointcnn: 3d object proposal generation and detection from point cloud. In *Proceedings of the IEEE/CVF conference on computer vision and pattern recognition*, pages 770–779, 2019. 2

[38] Shaoshuai Shi, Zhe Wang, Jianping Shi, Xiaogang Wang, and Hongsheng Li. From points to parts: 3d object detection from point cloud with part-aware and part-aggregation network. *IEEE transactions on pattern analysis and machine intelligence*, 43(8):2647–2664, 2020. 7

[39] Weijing Shi and Raj Rajkumar. Point-gnn: Graph neural network for 3d object detection in a point cloud. In *Proceedings of the IEEE/CVF conference on computer vision and pattern recognition*, pages 1711–1719, 2020. 2, 4, 5, 6, 7, 13, 14

[40] Michael Tschannen, Josip Djolonga, Marvin Ritter, Aravindh Mahendran, Neil Houlsby, Sylvain Gelly, and Mario Lucic. Self-supervised learning of video-induced visual invariances. In *Proceedings of the IEEE/CVF Conference on Computer Vision and Pattern Recognition*, pages 13806–13815, 2020. 1

[41] Sundar Vedula, Peter Rander, Robert Collins, and Takeo Kanade. Three-dimensional scene flow. *IEEE transactions on pattern analysis and machine intelligence*, 27(3):475–480, 2005. 2

[42] Christoph Vogel, Konrad Schindler, and Stefan Roth. 3d scene flow estimation with a piecewise rigid scene model. *International Journal of Computer Vision*, 115(1):1–28, 2015. 2

[43] Sourabh Vora, Alex H Lang, Bassam Helou, and Oscar Beijbom. Pointpainting: Sequential fusion for 3d object detection. In *Proceedings of the IEEE/CVF conference on computer vision and pattern recognition*, pages 4604–4612, 2020. 8

[44] Guojun Wang, Bin Tian, Yunfeng Ai, Tong Xu, Long Chen, and Dongpu Cao. Centernet3d: An anchor free object detector for autonomous driving. *arXiv preprint arXiv:2007.07214*, 2020. 7

[45] Guangming Wang, Xinrui Wu, Zhe Liu, and Hesheng Wang. Hierarchical attention learning of scene flow in 3d point clouds. *IEEE Transactions on Image Processing*, 30:5168–5181, 2021. 2

[46] Jun Wang, Shiyi Lan, Mingfei Gao, and Larry S Davis. Info-focus: 3d object detection for autonomous driving with dynamic information modeling. In *European Conference on Computer Vision*, pages 405–420. Springer, 2020. [8](#)

[47] Rui Wang, Nan Yang, Jörg Stückler, and Daniel Cremers. Directshape: Direct photometric alignment of shape priors for visual vehicle pose and shape estimation. In *2020 IEEE International Conference on Robotics and Automation (ICRA)*, pages 11067–11073. IEEE, 2020. [2](#)

[48] Xiaolong Wang and Abhinav Gupta. Unsupervised learning of visual representations using videos. In *Proceedings of the IEEE international conference on computer vision*, pages 2794–2802, 2015. [2](#)

[49] Xiaolong Wang, Allan Jabri, and Alexei A Efros. Learning correspondence from the cycle-consistency of time. In *Proceedings of the IEEE/CVF Conference on Computer Vision and Pattern Recognition*, pages 2566–2576, 2019. [2](#)

[50] Zirui Wang, Shuda Li, Henry Howard-Jenkins, Victor Prisacariu, and Min Chen. Flownet3d++: Geometric losses for deep scene flow estimation. In *Proceedings of the IEEE/CVF Winter Conference on Applications of Computer Vision*, pages 91–98, 2020. [2](#)

[51] Yi Wei, Ziyi Wang, Yongming Rao, Jiwen Lu, and Jie Zhou. Pv-raft: Point-voxel correlation fields for scene flow estimation of point clouds. In *Proceedings of the IEEE/CVF Conference on Computer Vision and Pattern Recognition*, pages 6954–6963, 2021. [2](#)

[52] Wenzuan Wu, Zhiyuan Wang, Zhuwen Li, Wei Liu, and Li Fuxin. Pointpwc-net: A coarse-to-fine network for supervised and self-supervised scene flow estimation on 3d point clouds. *arXiv preprint arXiv:1911.12408*, 2019. [2](#)

[53] Saining Xie, Jiatao Gu, Demi Guo, Charles R Qi, Leonidas Guibas, and Or Litany. Pointcontrast: Unsupervised pre-training for 3d point cloud understanding. In *European conference on computer vision*, pages 574–591. Springer, 2020. [2](#)

[54] Yan Yan, Yuxing Mao, and Bo Li. Second: Sparsely embedded convolutional detection. *Sensors*, 18(10):3337, 2018. [2](#), [6](#), [7](#)

[55] Zetong Yang, Yanan Sun, Shu Liu, and Jiaya Jia. 3dssd: Point-based 3d single stage object detector. In *Proceedings of the IEEE/CVF conference on computer vision and pattern recognition*, pages 11040–11048, 2020. [2](#)

[56] Zetong Yang, Yanan Sun, Shu Liu, Xiaoyong Shen, and Jiaya Jia. Std: Sparse-to-dense 3d object detector for point cloud. In *Proceedings of the IEEE/CVF International Conference on Computer Vision*, pages 1951–1960, 2019. [2](#)

[57] Maosheng Ye, Shuangjie Xu, and Tongyi Cao. Hvnet: Hybrid voxel network for lidar based 3d object detection. In *Proceedings of the IEEE/CVF conference on computer vision and pattern recognition*, pages 1631–1640, 2020. [2](#)

[58] Tianwei Yin, Xingyi Zhou, and Philipp Krahenbuhl. Center-based 3d object detection and tracking. In *Proceedings of the IEEE/CVF conference on computer vision and pattern recognition*, pages 11784–11793, 2021. [4](#), [7](#), [8](#), [9](#), [13](#), [14](#)

[59] Zhichao Yin and Jianping Shi. Geonet: Unsupervised learning of dense depth, optical flow and camera pose. In *Proceedings of the IEEE conference on computer vision and pattern recognition*, pages 1983–1992, 2018. [2](#)

[60] Dingfu Zhou, Jin Fang, Xibin Song, Liu Liu, Junbo Yin, Yuchao Dai, Hongdong Li, and Ruigang Yang. Joint 3d instance segmentation and object detection for autonomous driving. In *Proceedings of the IEEE/CVF Conference on Computer Vision and Pattern Recognition*, pages 1839–1849, 2020. [7](#)

[61] Yin Zhou and Oncel Tuzel. Voxelnet: End-to-end learning for point cloud based 3d object detection. In *Proceedings of the IEEE conference on computer vision and pattern recognition*, pages 4490–4499, 2018. [2](#), [6](#)

[62] Xinge Zhu, Yuexin Ma, Tai Wang, Yan Xu, Jianping Shi, and Dahua Lin. Ssn: Shape signature networks for multi-class object detection from point clouds. In *European Conference on Computer Vision*, pages 581–597. Springer, 2020. [13](#), [15](#)

[63] Yuliang Zou, Zelun Luo, and Jia-Bin Huang. Df-net: Unsupervised joint learning of depth and flow using cross-task consistency. In *Proceedings of the European conference on computer vision (ECCV)*, pages 36–53, 2018. [2](#)

# Appendices

## A. Point-GNN [39] Alternating Training Ablation

We compare Point-GNN 3D detector pre-trained with and without alternating training in Table 10 to justify our training strategy. The alternating training strategy repeats the self-supervised backbone training followed by the supervised 3D detection fine-tuning pair several times. We repeat the pair-wise training twice to get alternating training results. The *Self-sup Point-GNN* in Table 10 applies the pair-wise training (self-supervised followed by supervised) only once. For comparison purposes, we also include Point-GNN baseline results in this table. The alternating training strategy enhances the Car class 3D detection precision for more than 2% AP in the moderate difficulty level.

## B. Ablation on the nuScenes Dataset: Limited Labeled Data and Alternating Training

We further investigate our self-supervised scene flow pre-training method with CenterPoint[58], PointPillars[21], and SSN[62] 3D detectors on nuScenes dataset.

Fig. 6 shows the CenterPoint mAP and NDS 3D detection scores for training from scratch and using our pre-training method. We show the percentage of the training set used for supervised training in the x-axes. The blue lines indicate the baseline CenterPoint trained from scratch. We show the self-supervised CenterPoint results with orange lines (Ours\_a) without alternating training and green lines (Ours\_b) with alternating training. As seen, our pre-training enhances the 3D detection scores compared to the baseline, and the alternating training strategy further improves the results.

We show the 3D detection results (mAP and NDS) of the baseline and our self-supervised PointPillars in Fig 7. Blue lines give the baseline PointPillars trained with the given percentages of the labeled data. Ours\_a and Ours\_b belong to our self-supervised PointPillars without and with alternating training, respectively. The PointPillars obtained apparent improvements over the baseline based on our self-supervised pre-training approach.

We draw similar curves for the SSN 3D detector<sup>4</sup> trained with a part of annotated nuScenes 3D detection training split in Fig. 8. Blue lines are for the baseline SSN. Ours\_a and Ours\_b show the SSN 3D detection scores pre-trained without and with alternating training strategy. Our alternating self-supervised pre-training strategy improves the 3D mAP and NDS with a large margin compared to the baseline.

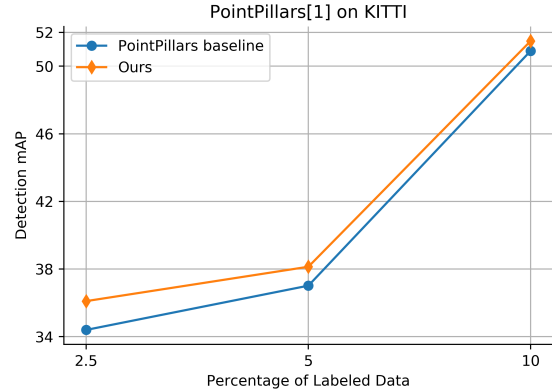


Figure 5: 3D detection results using PointPillars [21] trained with a small part of KITTI data. Ours (orange) is pre-trained with our self-supervised scene flow. Baseline (blue) is trained with the labeled data from scratch. Our pre-trained PointPillars outperforms the baseline trained with the limited labeled data.

## C. PointPillars [21] Ablation on KITTI: Limited Labeled Data

We compare our pre-training with the baseline using PointPillars trained with a small part of training split in Fig. 5 in addition to the PointPillars 3D detection results on nuScenes dataset given in the main paper. Blue and orange lines are for the baseline and our pre-trained PointPillars, respectively. The y-axis shows the mAP scores for all three classes on moderate difficulty level. As seen in the figure, our self-supervised pre-training provides better 3D detection mAP than training from scratch.

## D. Conclusion

Further ablation study results in this supplementary material suggest that our self-supervised scene flow pre-training helps achieve better 3D detection accuracy for several 3D detectors on KITTI and nuScenes datasets. Learning motion representations with the scene flow pre-training is especially useful when the annotated dataset is limited. Moreover, our alternating training strategy contributes to learning the relation between motion and geometric point cloud features, resulting in better 3D detection. We share our anonymized code in the supplementary material zip file.

<sup>4</sup><https://github.com/open-mmlab/mmdetection3d/>

Car (IoU=0.7)		3D AP			BEV AP		
Method		Easy	Mod	Hard	Easy	Mod	Hard
Point-GNN baseline [39]		90.44	82.12	77.70	93.03	89.31	86.86
Self-sup. Point-GNN		91.05	82.35	77.80	93.43	89.59	87.03
<b>Self-sup. Point-GNN w/ alternating tr.</b>		<b>91.43</b>	<b>82.85</b>	<b>80.12</b>	<b>93.55</b>	<b>89.79</b>	<b>87.23</b>

Table 10: Ablation results for applying the self-supervised training alternating with the 3D detection fine-tuning.

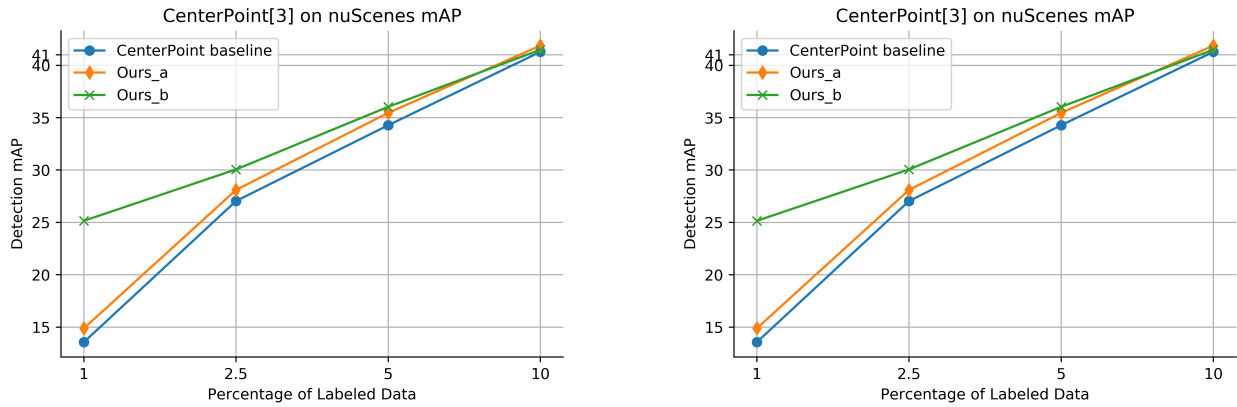


Figure 6: CenterPoint [58] 3D detection ablation results on the nuScenes dataset. All the CenterPoint versions are trained with the given percentage of the labeled data in the x-axes. The baseline (blue line) indicates training from scratch. Ours\_a (orange) and Ours\_b (green) are without and with alternating training. Our self-supervised pre-training enhances nuScenes 3D detection scores (mAP and NDS) compared to the baseline.

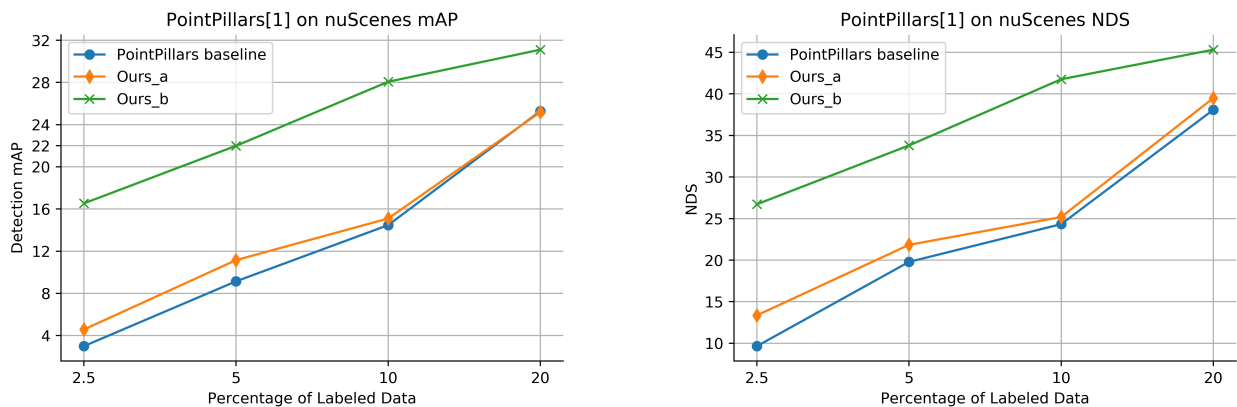


Figure 7: PointPillars[21] 3D detection ablation results on the nuScenes dataset. All the PointPillars versions are trained with a part of labeled data shown in the x-axis. The baseline (blue) was trained with labeled data from scratch. Our self-supervised approaches Ours\_a without alternating training and Ours\_b with alternating training outperform the baseline on mAP and NDS metrics significantly.

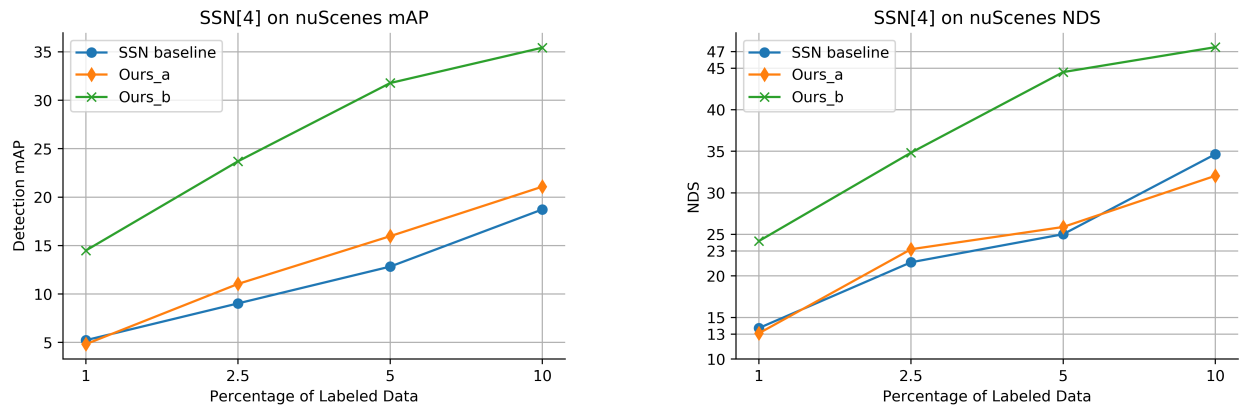


Figure 8: SSN[62] 3D detection ablation results on the nuScenes dataset. We trained the baseline (blue) with the labeled data from scratch. Ours\_a (without alternating training) and Ours\_b (with alternating training) are pre-trained with our self-supervised scene flow method and then trained with the labeled data. All the SSN versions are trained with the indicated percentage of the labeled data in the x-axis. Our pre-trained SSN outperforms the baseline on mAP and NDS metrics.